Applied Catalysis B: Environmental 170-171 (2015) 53–65

Contents lists available at ScienceDirect

Applied Catalysis B: Environmental

journal homepage: www.elsevier.com/locate/apcatb

Nanostructured TiO_2/KIT-6 catalysts for improved photocatalytic reduction of CO_2 to tunable energy products

Murid Hussain[a,b], Parveen Akhter[a], Guido Saracco[a], Nunzio Russo[a,*]

[a] Department of Applied Science and Technology, Politecnico di Torino, Corso Duca degli Abruzzi 24, 10129 Torino, Italy
[b] Department of Chemical Engineering, COMSATS Institute of Information Technology, M.A. Jinnah Building, Defence Road, Off Raiwind Road, Lahore 54000, Pakistan

ARTICLE INFO

Article history:
Received 10 November 2014
Received in revised form 7 January 2015
Accepted 9 January 2015
Available online 21 January 2015

Keywords:
Titania–silica catalysts
Photocatalysis
CO_2 reduction
Water vapor
Fuel

ABSTRACT

Nanostructured TiO_2/KIT-6 catalysts with different concentrations of incorporated TiO_2, have been synthesized, characterized, and examined in order to improve the photocatalytic reduction of carbon dioxide (CO_2) feedstock with water vapor (H_2O) to produce tunable value-added energy products. Nanostructured TiO_2, dispersed on KIT-6 (three-dimensional mesoporous silica), was found to be present in both the silica framework and on the surface, where it produced large surface area photocatalysts with enhanced adsorption capability of the reactants to photocatalytically convert into CH_4, CH_3OH (hydrocarbons) and CO, H_2 (similar to syngas). The formed products were influenced directly by the dispersed TiO_2 concentration as well as by the calcination temperature. Hydrocarbon and CO formation as well as the reaction kinetics improved as the TiO_2 concentration was increased from 1 to 20 wt%. However, a further increase in TiO_2 loadings (to 90%) decreased the hydrocarbon and CO, and increased H_2 formation. The highest optimization toward hydrocabon selectivity was shown by 20 wt% TiO_2, while a 90 wt% TiO_2 loading was more selective for H_2 formation. This was likely due to the uniform dispersion and stabilization of the anatase TiO_2 with 20 wt% on KIT-6, which in turn allowed more CO_2 adsorption and a better light penetration than 90% TiO_2/KIT-6 in which it showed a bulk phase and large agglomerates with light penetration limitations that were more favorable for H_2O adsorption. A reaction mechanism, which has helped to understand these findings, has been proposed. Moreover, a 24 h activity test with the optimized 20 wt% TiO_2/KIT-6 showed an increase in the product yield but only a minor, gradual decrease in the reaction rate, which points out that these photocatalysts could be promising for turning CO_2 greenhouse gas feedstock into selective renewable energy products.

1. Introduction

Carbon dioxide (CO_2), the most abundant and primary greenhouse gas, is currently a key global challenge [1,2]. The recent atmospheric concentration trend of CO_2, which mainly arises from human activities such as fossil fuel combustion in transport and energy production, plays a key role in global warming and has led to a great deal of environmental concern about human activities [3–5]. Moreover, due to the remarkable increase in human activities, a huge demand for energy has been generated. In this scenario, shortages and restrictions on the use of fossil fuels have emerged. The ever-increasing energy demand has led to the proposal of using CO_2 as a raw material to produce alternative energy products in order to satisfy future needs [6,7].

Carbon capture and sequestration (CCS) is surely a useful way of effectively controlling the greenhouse effect [5,8,9]. However, converting CO_2 to value-added energy products is not only a promising way of tackling the greenhouse effect issue, but also a very useful way of producing alternative fuels to solve the energy crisis [6,10]. Therefore, a research trend in this direction has recently been observed to tackle this issue [1,2,4,6–8,10,11]. Photovoltaic cells, photoelectrochemical cells, direct photocatalytic reduction using molecular catalysts and photocatalytic reduction through water are but a few of those techniques that are being studied intensively in this direction [6]. CO_2 is an inert and thermodynamically very stable molecule which is difficult to decompose under ambient reaction conditions. However, since the first report by Inoue et al. [11] the photocatalytic reduction of CO_2 with water vapor has become one of the most promising techniques to convert CO_2 to useful energy products or basic chemical raw-materials, such as methane (CH_4), methanol (CH_3OH), carbon monoxide (CO), formic acid (HCOOH), formaldehyde (HCHO), etc. [2,8,12–22]. However, the lower effi-

* Corresponding author. Tel.: +39 011 0904710; fax: +39 011 0904699.
E-mail address: nunzio.russo@polito.it (N. Russo).

http://dx.doi.org/10.1016/j.apcatb.2015.01.007
0926-3373/

ciency of this technology is a major barrier to this process which is still in an embryonic stage and has not yet been commercialized.

Oxide and nonoxide photocatalysts have been explored extensively from the photocatalytic reduction point of view, to produce various energy-bearing products [1]. Of all these materials, TiO_2 photocatalysts with a band gap energy of 3.2 eV have been shown to be the most convenient candidates for this application, due to their charge carrier properties. However, their lower catalytic efficiency and product selectivity are the key challenges to CO_2 conversion for fuel applications. For these reasons, there has been a huge effort in this area to develop highly efficient and promising catalysts for improved selective products.

Various techniques, including synthesis of the uniform single-phase titania crystalline structure, band-gap modification of the UV-activated TiO_2 particles, surface cocatalyst deposition to catalyze redox reactions, the use of a sensitization effect to harness visible light, and enhancing nanofabrication techniques to obtain a better control of the size and morphology, are currently being explored to develop more efficient TiO_2-based photocatalysts in order to convert CO_2 into fuels or chemicals. However, in most of these cases, the used TiO_2 was present in the bulk phase in which a lower specific surface area of the photocatalysts is available for the reactants to adsorb in the gas phase reaction, as well as light (UV or visible) penetration limitations in the bulk phase. These disadvantages have led to a low photocatalytic conversion of CO_2 as well as photocatalyst deactivation issues [1,19].

In order to tackle these issues, highly dispersed titanium oxide (Ti-oxide) catalysts anchored on porous Vycor glass, zeolites and some nanoporous silica materials, such as MCM-41, SBA-15, and KIT-6, have been studied to obtain better photocatalytic activity, than the bulk TiO_2 powder, for CO_2 conversion [12,17,23]. Mesoporous silica materials with a combination of good accessibility, uniform pore size and high surface area, have been explored as supports to provide a better dispersion of the active isolated-Ti phase with the aim of increasing the overall area of the photocatalyst. However, in these types of supported isolated-Ti photocatalysts, there are strong, stable but very limited active sites, which are very quickly consumed and this causes a rapid deactivation of the photocatalysts.

KIT-6, an interesting mesoporous silica support with a 3-dimensional (3D, large-pore gyroid cubic Ia3d) pore structure, has already received the attention of many researchers for various other applications [24–26]. In the present work, an attempt has been made to synthesize KIT-6 supported TiO_2 nanostructured photocatalysts in order to a obtain better dispersed active TiO_2 phase with an enhanced surface area so as to achieve a better adsorption of the reactants for the reaction to enhance photocatalytic activity, without any co-particle, noble metal, or sacrificial reagent. A better dispersed active phase could reduce the light penetration limitations that are present in the bulk TiO_2 phase. This could increase the catalytic activity and improve the stability of the photocatalyst. These nanostructured TiO_2/KIT-6 photocatalysts have been synthesized and characterized by means of X-ray diffraction (XRD), N_2-sorption, field emission scanning electron microscope (FE-SEM), Ultraviolet–visible (UV–vis) spectroscopy, scanning transmission electron microscopy (STEM) and X-ray photoelectron spectroscopy (XPS) analysis techniques to explore their characteristics and eventually were applied for the photocatalytic reduction of CO_2 with H_2O vapor to obtain various energy-bearing products (CH_4, CH_3OH, CO, and H_2). Different TiO_2 loadings (1–90 wt%) on KIT-6, have been examined in this work, and various energy-bearing products have been produced with different selectivity. A correlation has been found between the properties and the activity results.

2. Experimental

2.1. Synthesis of the nanostructured TiO_2/KIT-6 photocatalysts

KIT-6 mesoporous silica material has been synthesized according to the hydrothermal treatment procedure that has been used in recent works [24–26]. The final obtained solid product was filtered, dried and calcined at 550 °C for 5 h for further use in the synthesis of KIT-6 incorporated TiO_2 photocatalysts.

The nanostructured TiO_2/KIT-6 photocatalyst was prepared by means of sol–gel hydrolysis and condensation of an isopropanol solution of titanium tetraisopropoxide (TTIP, Sigma–Aldrich, 98%) in the presence of the synthesized KIT-6 support material [27]. Hydrochloric acid (HCl) was added to the TTIP solution to prevent hydrolysis and precipitation before KIT-6 was added. KIT-6 was then added to the TTIP solution and all the reactants were mixed thoroughly. This was followed by the addition of H_2O. In order to synthesize the nanostructured TiO_2/KIT-6 photocatalysts with different TiO_2 loadings, the required TTIP amount in isopropanol was incorporated in KIT-6 to achieve, 1, 5, 10, 20, 30, 50, 70, and 90 wt% TiO_2 dispersed on KIT-6. In each case, after intensive mixing, the solvent was evaporated from the mixture and the recovered solid product was dried at 80 °C overnight. The final products were calcined at 400 °C for 3 h. The optimized TiO_2 (20%)/KIT-6 was also calcined at 400–800 °C to obtain the most suitable condition for effective use.

2.2. Characterizations of the nanostructured TiO_2/KIT-6 photocatalysts

The XRD patterns of TiO_2/KIT-6 were recorded on an X'Pert Phillips diffractomer, using Cu Kα radiation, under the conditions of 2θ = 10–90° and 2θ step size = 0.02, in order to examine the different polymorphs.

The Brunauer–Emmett–Teller (BET) specific surface area (S_{BET}), pore volume (PV), average pore diameter (APD) and isotherms were measured on the powder materials. Before analysis, the materials were outgassed at 150 °C using a Micromeritics FlowPrep 060, USA. An N_2 sorption analysis was performed at 77 K on a Micromeritics Tristar II, USA (surface area and porosity) instrument.

The morphology and mesoporous structure of the materials were observed by means of a Zeiss Merlin FE-SEM instrument. The UV–vis diffuse reflectance spectra were obtained using a Varian model Cary 500 spectrophotometer, with a quartz cell suitable for the measurement of powder materials.

The XPS spectra were recorded using a PHI 5000 Versa Probe (USA), which included a scanning ESCA microscope fitted with an Al monochromatic X-ray source (1486.6 eV, 25.6 W). A beam diameter of 100 μm and a neutralizer at 1.4 eV, 20 mA, were used during the analysis in FAT analyzer mode. Zeiss Merlin STEM device with an EDAX detector (Oxford) was used to observe the mesoporosity and TiO_2 dispersed in KIT-6, using thin edges of the samples.

2.3. Photocatalytic reaction system

The set-up of the CO_2 photocatalytic reduction system is shown in Fig. S1 (Supplementary material). The system includes a Pyrex glass reactor (1.2 L of internal volume), connectors, mass flow controllers (Bronkhorst, High-Tech), a water bubbler, and a UV lamp (Osram Ultra-Vitalux 300 W). The reaction system also includes a He and a CO_2 (99.99%) gas cylinder. A gas chromatograph (GC, Varian CP-3800) equipped with a capillary column (CP7381, fused silica), a flame ionization detector (FID) and a thermal conductivity detector (TCD), was used for the analysis of the gas products during the reaction. A photocatalytic reaction was performed with 0.2 g of the photocatalyst in the reactor, which was dispersed on

Table 1
Physical properties, band gap energies and Ti/Si ratios comparison of the materials.

Samples	N_2-physisorption			UV–vis	Ti/Si molar ratios	
	S_{BET}	PV	APD	E	Theoretical	Actual by XPS
KIT-6Calcined	770	1.03	5.1	n.d.	n.d.	n.d.
TiO_2(1 wt%)/KIT-6	735	0.98	5.0	3.35	n.d.	n.d.
TiO_2(5 wt%)/KIT-6	702	0.83	4.9	3.25	0.031	0.030
TiO_2(10 wt%)/KIT-6	637	0.71	4.9	3.23	n.d.	n.d.
TiO_2(20 wt%)/KIT-6	563	0.68	4.9	3.15	0.147	0.140
TiO_2(30 wt%)/KIT-6	539	0.63	4.8	3.13	n.d.	n.d.
TiO_2(50 wt%)/KIT-6	431	0.52	4.7	3.11	0.587	0.495
TiO_2(70 wt%)/KIT-6	408	0.45	4.9	n.d.	0.730	0.602
TiO_2(90 wt%)/KIT-6	383	0.35	5.0	3.08	n.d.	n.d.
TiO_2(20 wt%)/KIT-6–400 °C	563	0.68	4.9	3.15	0.031	0.030
TiO_2(20 wt%)/KIT-6–500 °C	560	0.69	5.0	n.d.	n.d.	n.d.
TiO_2(20 wt%)/KIT-6–600 °C	540	0.67	5.0	n.d.	n.d.	n.d.
TiO_2(20 wt%)/KIT-6–700 °C	503	0.65	5.2	n.d.	n.d.	n.d.
TiO_2(20 wt%)/KIT-6–800 °C	454	0.60	5.3	n.d.	n.d.	n.d.

S_{BET} – BET specific surface area in m^2/g; PV – cumulative pore volume in cm^3/g; APD – average pore diameter in nm; E – band gap energy, eV; n.d. – not determined.

a Pyrex glass substrate within the reactor. The trapped air and the impurities in the reactor and lines were removed by purging a He flow. Then a 50 mL flow of 20% CO_2 (after diluting with He) was introduced into the reactor, after passing it through the water bubbler and ensuring it was adsorption–desorption balanced in order to saturate the catalyst with CO_2 and H_2O vapors. The reaction was started as equilibrium was reached, by turning on the UV light. The reaction products were continuously analyzed by means of the GC aforementioned. In order to confirm that the produced reaction products were due to a photocatalytic reaction, blank tests involving UV-illumination without the photocatalyst, and a reaction in the dark with the photocatalyst were conducted.

3. Results and discussion

3.1. Physico-chemical properties of the nanostructured TiO_2/KIT-6 photocatalysts

Modern, highly efficient catalysts are made of materials that usually have high surface areas with nanometric sized particles,

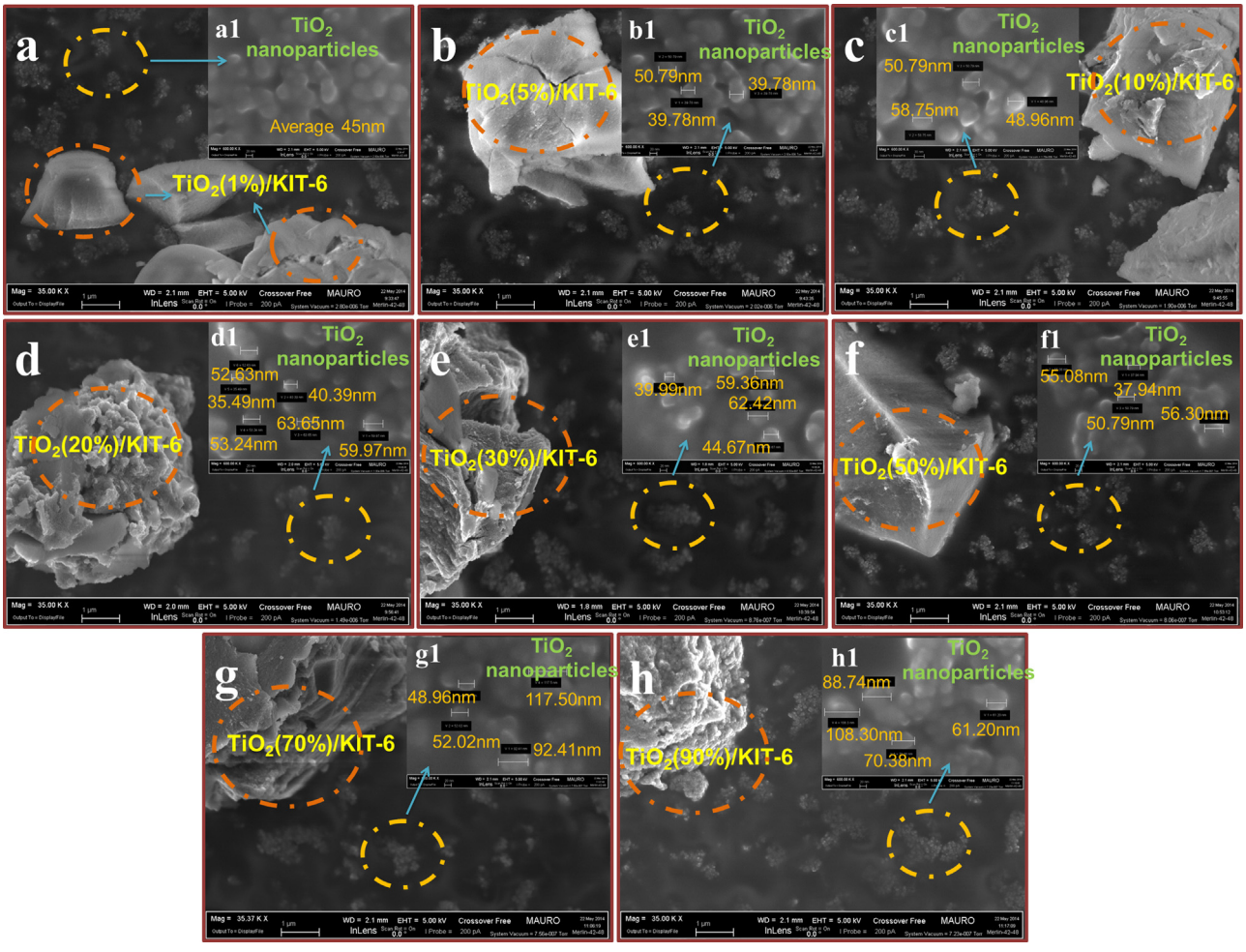

Fig. 1. FE-SEM images of TiO_2(x)/KIT-6 photocatalysts: x indicates (a) 1; (b) 5; (c) 10; (d) 20; (e) 30; (f) 50; (g) 70; and (h) 90%.

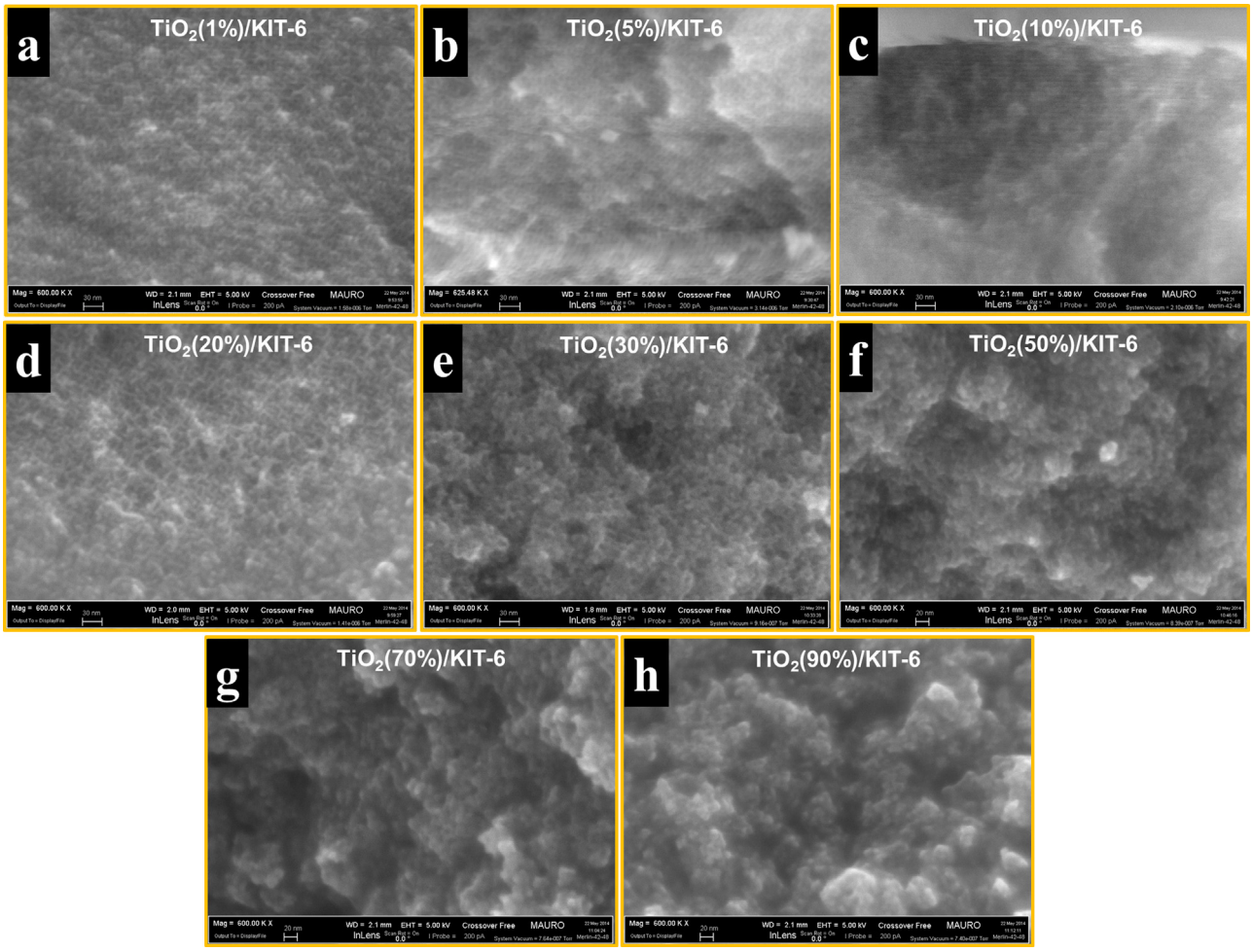

Fig. 2. High resolution FE-SEM images of $TiO_2(x)$/KIT-6 photocatalysts: *x* indicates (a) 1; (b) 5; (c) 10; (d) 20; (e) 30; (f) 50; (g) 70; and (h) 90%.

normally below 100 nm [28,29]. Recent in-depth analyses have shown that the size, shape, and porosity of the particles are the key morphological parameters that can influence their photoactivity. Therefore, a decrease in the particle size of a uniformly dispersed active phase on a highly-ordered porous support material would provide a high surface area photocatalyst and this would generally have a beneficial effect on photoactivity [1,28]. Therefore, particular attention has been paid in this study to obtaining nano-sized TiO_2 dispersed on 3D ordered porous KIT-6 silica material, in order to enhance CO_2 conversion to fuel and other useful energy-bearing products. The physical characteristics of these synthesized photocatalysts have been obtained by means of N_2-sorption, and are summarized in Table 1. KIT-6 has a high surface area (S_{BET}), pore volume (PV), and confined 3D average pore diameter (APD), which are shown in Table 1. As the TiO_2 loading was increased, a gradual decrease was observed in the S_{BET} and PV of the KIT-6 support material. This decrease was due to partial surface coverage and blockage by the dispersed TiO_2. However, because of the 3D pore structure of KIT-6, a uniform APD was observed in all the catalysts (calcined at 400 °C for 3 h), which did not change significantly. The 3D pore structure was able to accommodate dispersed TiO_2 and facilitate an easier and faster diffusion of the reactants and products [25]. Therefore, the TiO_2 loadings on KIT-6 were uniform up to 20–30%, while loadings above this decreased the physical characteristics significantly. Different temperature calcination treatments of TiO_2(20%)/KIT-6 (ranging 400–800 °C) also showed a decrease in S_{BET} and PV, which might have been caused by the rapid growth of TiO_2 due to sintering, and in particular inside the KIT-6 pores.

According to the definition of the International Union of Pure and Applied Chemistry (IUPAC), KIT-6 shows a typical reversible type IV adsorption/desorption isotherm, which also provides very interesting information, through its hysteresis loop, regarding the mesoporous structure [30,31]. Fig. S2 shows the isotherms of TiO_2(1–90%)/KIT-6 (calcined at 400 °C/3 h) and TiO_2(20%)/KIT-6 calcined at different temperatures, ranging from 400 to 800 °C, for 3 h. As shown in Fig. S2(a), the adsorption branch of each isotherm in TiO_2(1–90%)/KIT-6 showed a sharp inflection in the 0.5–0.8 relative pressure range, which means a typical capillary condensation within the uniform pores with a typical H1 type hysteresis loop, which indicates large channel like pores with a confined pore size distribution. A gradual decrease was observed in the volume adsorbed by the increased TiO_2 content dispersed on KIT-6, in agreement with the BET results shown in Table 1. However, the hysteresis positions and shapes were preserved in all the TiO_2/KIT-6 photocatalysts. A similar trend was observed regarding TiO_2(20%)/KIT-6 (calcined at 400, 800 °C for 3 h), shown in Fig. S2(b), a result that is also consistent with the previously described S_{BET} and PV data trend.

The phase composition of TiO_2(1–90%)/KIT-6 and TiO_2(20%)/KIT-6 (calcined at 400–800 °C) was obtained from XRD patterns and is shown in Fig. S3. Recent analyses have indicated that anatase shows more activity than rutile, in most photocatalytic reaction systems [32]. The enhancement in photoac-

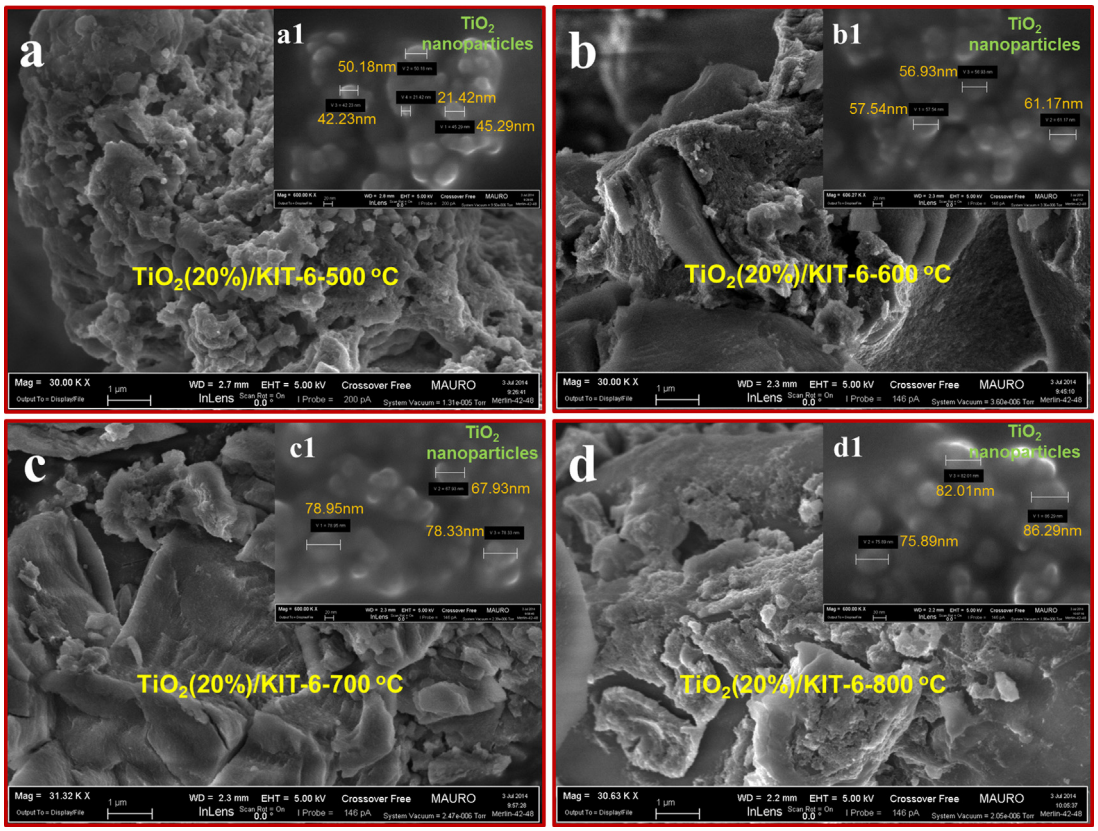

Fig. 3. FE-SEM images of TiO_2(20%)/KIT-6 photocatalysts calcined at: (a) 500 °C; (b) 600 °C; (c) 700 °C; and (d) 800 °C.

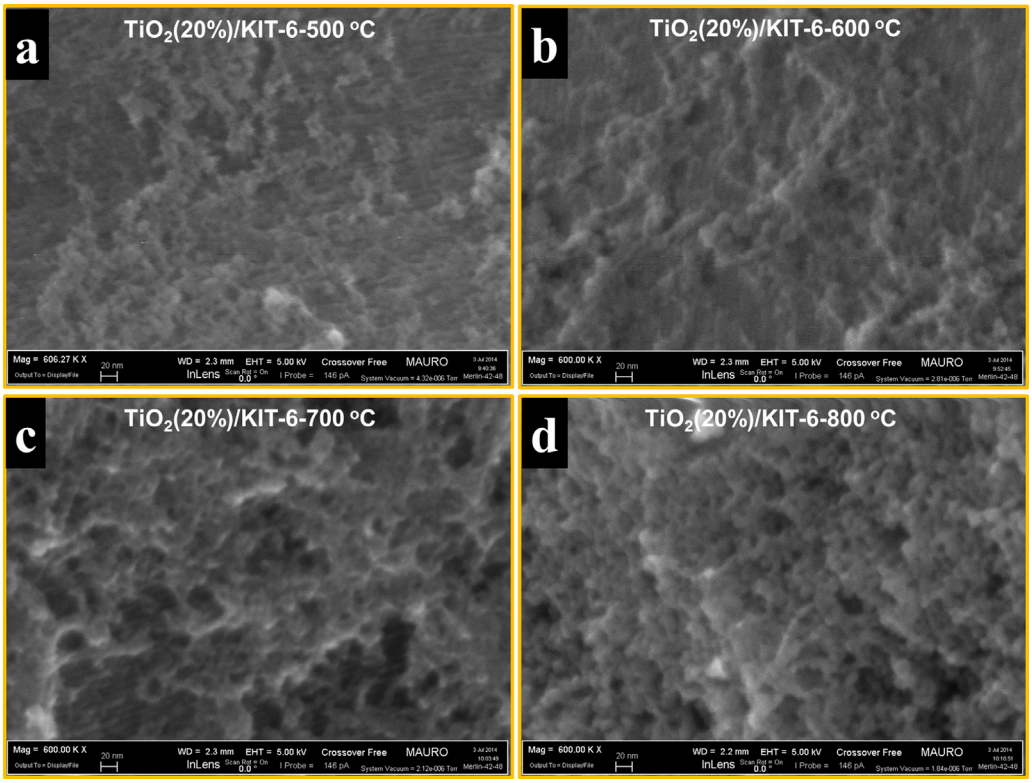

Fig. 4. High resolution FE-SEM images of TiO_2(20%)/KIT-6 photocatalysts calcined at: (a) 500 °C; (b) 600 °C; (c) 700 °C; and (d) 800 °C.

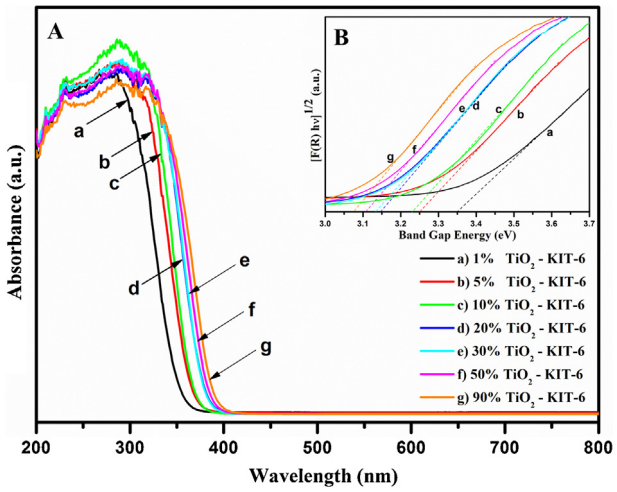

Fig. 5. UV–vis spectra of $TiO_2(x)$/KIT-6 photocatalysts: x indicates (a) 1; (b) 5; (c) 10; (d) 20; (e) 30; (f) 50; and (g) 90%.

tivity has been considered to be due to the fact that the Fermi level of anatase is higher than that of rutile, while rutile is usually less active, due to the fast recombination of e^- and h^+ [33]. Therefore, the key goal of this work is the highly dispersed TiO_2 anatase phase.

The XRD peaks were identified by the following Cards (Anatase: 89–4921, Rutile: 89–4920, Aluminum (sample holder): 04–0787). As can be seen in Fig. S3(a), the amorphous silica peak at a 2-theta value of 23 gradually disappeared, and anatase phase peaks appeared due to increased TiO_2 loadings from 1 to 90%. However, as the TiO_2 loading was increased to more than 20%, the anatase phase has been still found dominant in all the samples.

Fig. S3(b) shows only a small indication of anatase to rutile phase transformation due to increased calcination temperatures from 400 to 800 °C. Besides the phase transformation, the high calcination temperatures also induced an undesired sintering of TiO_2.

The morphology of different TiO_2 loadings dispersed on KIT-6 has been established through FE-SEM analysis, and is shown in Fig. 1. These images indicate that the incorporated TiO_2 was dispersed on the KIT-6 support material and was also present in the small agglomerates in nanoparticle form. Fig. 1a–h shows that TiO_2 is well dispersed on KIT-6 for lower TiO_2 loadings, and then gradually shows agglomerates as the TiO_2 loadings are increased up to 90%. It has also been observed that the size of these TiO_2 nanoparticles and agglomerates gradually became larger with an increase in the TiO_2 loadings from 1 to 90%; this is clearly shown in Fig. 1a1–h1.

The high resolution FE-SEM images of the TiO_2(1–90%)/KIT-6 photocatalysts shown in Fig. 2a–h, show the TiO_2 dispersion on the KIT-6 support materials. The 1–20% TiO_2 dispersion is comparatively uniform, with less agglomerate formation, and the KIT-6 mesostructure can be observed. However, an increased TiO_2 loading of 30–90% shows a gradual and larger agglomerate formation, until the KIT-6 support material is covered completely.

Similar agglomeration and sintering phenomena have been observed and are shown in Figs. 3 and 4, when the TiO_2(20%)/KIT-6 photocatalysts were calcined at 500–800 °C for 3 h. As the calcination temperature was increased from 400 to 800 °C, a rapid growth in the particles from an average size of 40 to 80 nm was noticed

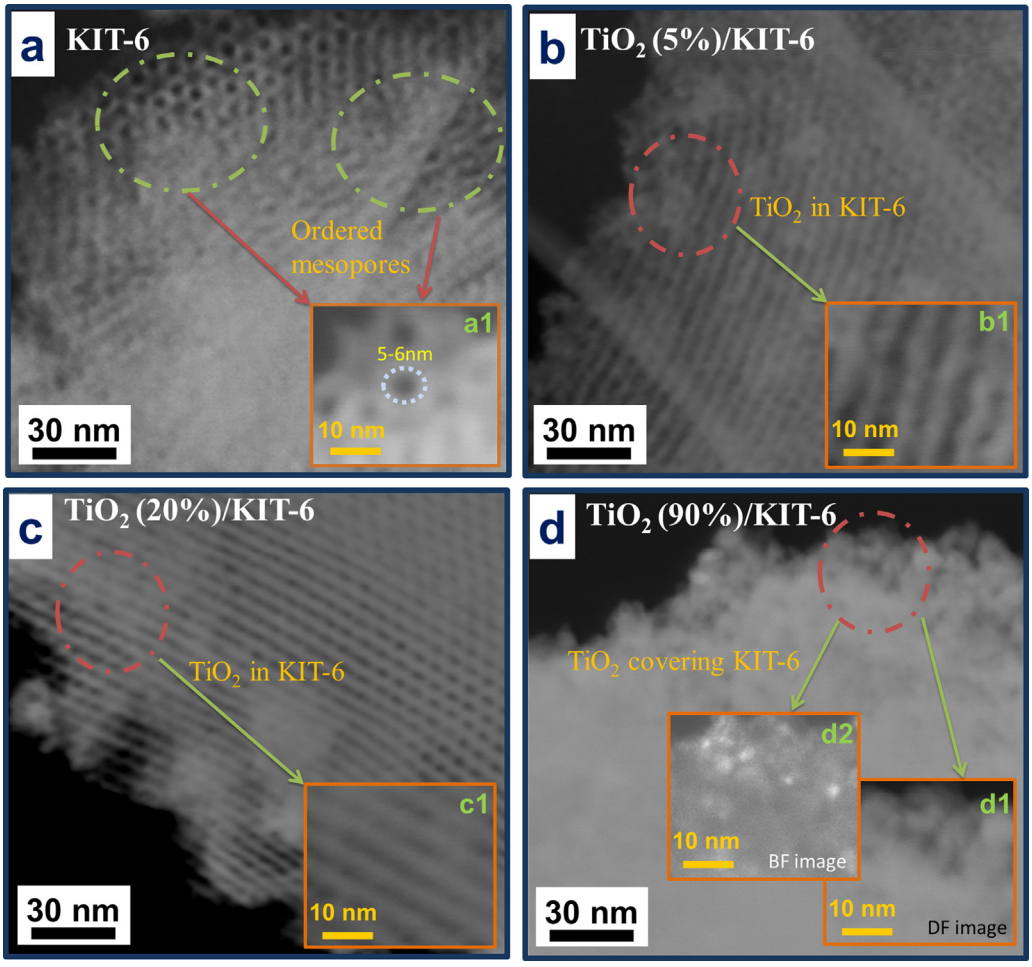

Fig. 6. STEM images of: (a) KIT-6; (b) TiO_2(5%)/KIT-6; (c) TiO_2(20%)/KIT-6; and (d) TiO_2(90%)/KIT-6 photocatalysts.

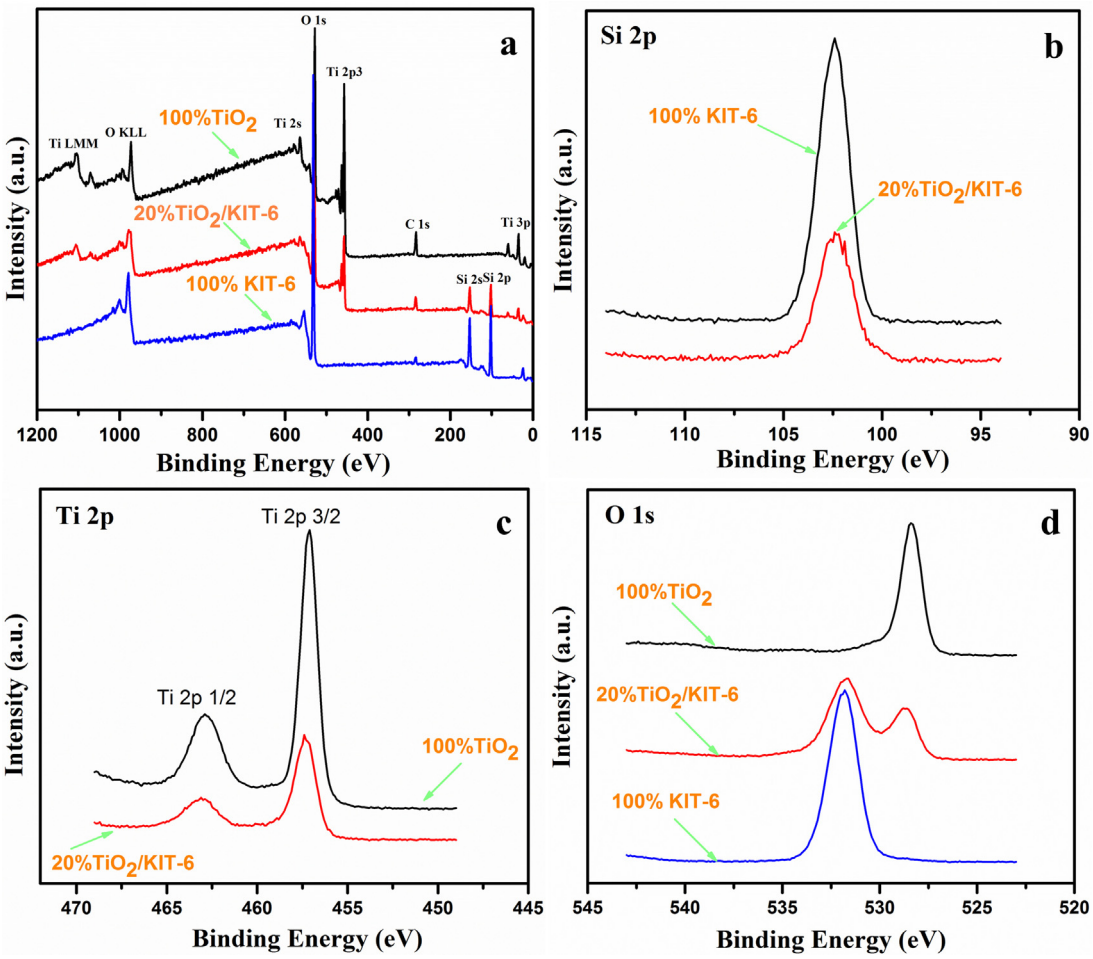

Fig. 7. XPS analysis of the materials: (a) overall scan; (b) Si 2p; (c) Ti 2p; and (d) O 1s spectra.

and can be observed in Fig. 3. This effect is more easily observed in the high resolution FE-SEM images shown in Fig. 4, where the TiO_2 particles seem to grow with increased temperature and have agglomerated with each other to form a thick film on the surface of KIT-6. Therefore, higher TiO_2 loadings and higher calcination temperatures do not seem to be the appropriate conditions to overcome the light penetration hurdle for photocatalytic applications.

The UV–vis spectra of the synthesized TiO_2(1–90%)/KIT-6 materials are shown in Fig. 5 and Table 1. UV–vis spectroscopy analysis is a useful technique that can provide important information on the interactions of photocatalytic materials with photon energies, in order to choose the proper light to activate semiconducting materials [34]. It has been observed that the absorption spectra of the materials were shifted towards higher wavelengths for increased TiO_2 loadings from 1 to 90%, as shown in Fig. 5A. The band gap energy calculations are shown in Fig. 5B, and the values are presented in Table 1. These values are in accordance with the band gap energy of pure TiO_2, i.e., 3.20 eV [35]. The small variation (3.35–3.08 eV) that can be observed in the band gap energies is due to the different TiO_2 loadings on KIT-6. However, the band gap energy of the photocatalytic materials indicated that all these were within the light range used for the photocatalytic reaction.

STEM has been used to observe the mesoporous structure of KIT-6 and the dispersion of TiO_2 within the structure and on the surface of the support material, which is shown in Fig. 6. The synthesized KIT-6 material that was used as a support for TiO_2 dispersion shows an ordered array of mesopores, as can be seen in Fig. 6a. It is obvious that the centers of two adjacent pores are about 10 nm apart, which indicates a pore diameter of about 5–6 nm, as shown in Fig. 6a1. These findings are consistent with those obtained from APD by N_2-sorption (Table 1) as well as with those present in the literature [25]. Fig. 6b–d shows selective TiO_2 loadings on KIT-6. It has been observed that TiO_2 was comparatively better dispersed within the structure and on the surface of the KIT-6 present in the monolayer until a loading of 20% TiO_2. However, at a high TiO_2 loading of 90%, it covered the whole surface of the support and was present in large agglomerates, like 100% bulk TiO_2. The overlapping of amorphous and anatase is obvious which is due to dominant bulk TiO_2 under these moderate and standard calcination conditions. The anatase peak becomes sharper at higher calcination temperatures. The aforementioned trend of TiO_2 on silica could be also correlated with the difference in Ti/Si ratios (theoretical vs. actual) obtained by XPS analysis of selective samples of this series, shown in Table 1.

Fig. 7a shows an overall comparison of the optimized TiO_2(20%)/KIT-6 (calcined at 400 °C/3 h) with 100% silica(KIT-6) and 100% TiO_2(Aeroxide P25 TiO_2, a reference) through XPS analysis; the composition and peak consistency in the 20% TiO_2 loading can be observed. Another comparison of these materials through Si 2p, Ti 2p, and O 1s XPS spectra, is shown in Fig. 7b–d. A single peak observed at 102.4 eV has been assigned to Si, due to the silica in 20% TiO_2/KIT-6, which shows less intensity than the 100% silica peak shown in Fig. 7b. Similarly, the peak at around 457 and the second peak at around 463 eV in Fig. 7c, represent Ti 2p, due to TiO_2, and have less intensity than the 100% TiO_2. However, as shown in Fig. 7d, there are 2 peaks for the 20% TiO_2/KIT-6 catalyst, unlike the

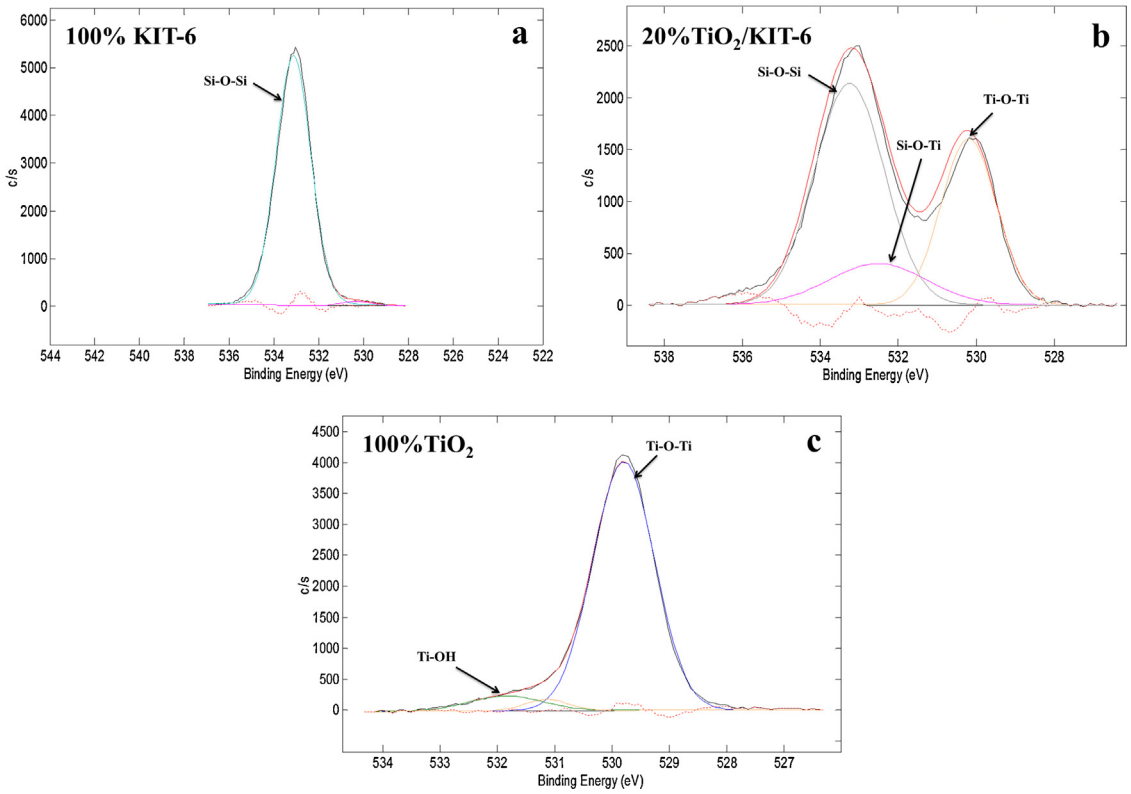

Fig. 8. XPS deconvoluted spectra of: (a) 100% KIT-6; (b) 20% TiO_2/KIT-6; and (c) 100% TiO_2 materials.

pure silica and pure titania. The first peak at around 533 eV is due to the oxygen from silica, whereas the second peak present at around 529.7 eV is caused by the oxygen from titania.

Other deconvoluted O 1s XPS spectra of the above described materials have been obtained to establish the nature of TiO_2 within the silica framework and present on the surface. Fig. 8 and Table 2 clearly show the oxygen present in pure silica, pure titania and 20% TiO_2/KIT-6 materials. All the oxygen in pure silica or titania is present in Si–O–Si and Ti–O–Ti form, except for any impurities or for the hydroxyl groups due to water. However, the fitting results of 20% TiO_2/KIT-6 photocatalyst show that, in addition to 2 peaks around 533, 529.7 eV, which have been assigned to Si–O–Si and Ti–O–Ti, respectively, there is another peak at around 532.2 eV that could be due to Si–O–Ti [27,36]. This indicates that TiO_2 is present in the 20% TiO_2/KIT-6 photocatalyst, in both the KIT-6 framework and on the surface.

3.2. Photocatalytic CO_2 reduction activity

A pretreatment was performed before the reaction by flushing a He flow through the reaction system lines, water bubbler and the reactor; this removed any trapped air or any other impurity within the reactor. Moreover, the blank activity tests were conducted without any photocatalyst as was the reaction in the dark with the catalyst. The results obtained have shown that there was no product formation during the blank activity tests (not shown in data for simplicity purpose), which indicates that all the products obtained during the reaction were produced by the photocatalysts.

Table 2
O 1s XPS fitting results for the 100% KIT-6, 20% TiO_2/KIT-6 and 100% TiO_2 materials.

Samples	O 1s				
	Si–O–Si (%)	Si–O–Ti (%)	Ti–O–Ti (%)	–OH(H_2O) (%)	Impurity (%)
100% KIT-6	99.8	0	0	0	0.2
20% TiO_2/KIT-6	53.9	14.1	32	0	0
100% TiO_2	0	0	94.6	5.4	0

The photocatalytic activity results for all the TiO_2(1–90%)/KIT-6 materials toward the conversion of CO_2 greenhouse gas with H_2O vapor into different renewable energy products are shown in Fig. 9. The main products that formed through the reaction were CH_4, CO, CH_3OH, H_2, and many other undetectable hydrocarbons. All of these products are useful energy-bearing ones, which can either be used directly as energy sources or used to produce other valuable chemicals or fuels [37]. However, CH_4 was considered the main desired product, due to its greater energy and heat content than H_2 or CO and H_2 (similar to syngas). Moreover, CH_3OH was only detected in the vapor phase and was not actual as produced or adsorbed by the powder photocatalyst.

Fig. 9 shows a comparison of the production rates of all the aforementioned products considering the CO_2 reduction with water vapor by the TiO_2(1–90%)/KIT-6 photocatalysts. It was observed that, as the TiO_2 loading was increased from 1 to 20%, the hydrocarbon (CH_4, CH_3OH) and CO formation rates also gradually increased. The TiO_2(20%)/KIT-6 photocatalyst showed the highest hydrocarbon and CO production rates, and are shown in Fig. 9d. However, a further increase in TiO_2 loadings on KIT-6 resulted in a gradual decrease in the hydrocarbon and CO production rates, but the H_2 production rate was found to be accelerated. Fig. 9h indicates that the TiO_2(90%)/KIT-6 photocatalyst generated the highest H_2 and the lowest hydrocarbon production rates.

Fig. 10 clearly shows the activity of the TiO_2(1–90%)/KIT-6 photocatalysts on the basis of the total production over a 5 h reaction time. The highest production can be observed for CH_4, CH_3OH, and CO (44.5568, 1.0871, 120.5447 μmol g cat.$^{-1}$, respectively, Fig. 10d) for the TiO_2(20%)/KIT-6 compared to all the other catalysts, whereas the highest H_2 production (154.5299 μmol g cat.$^{-1}$) was induced by

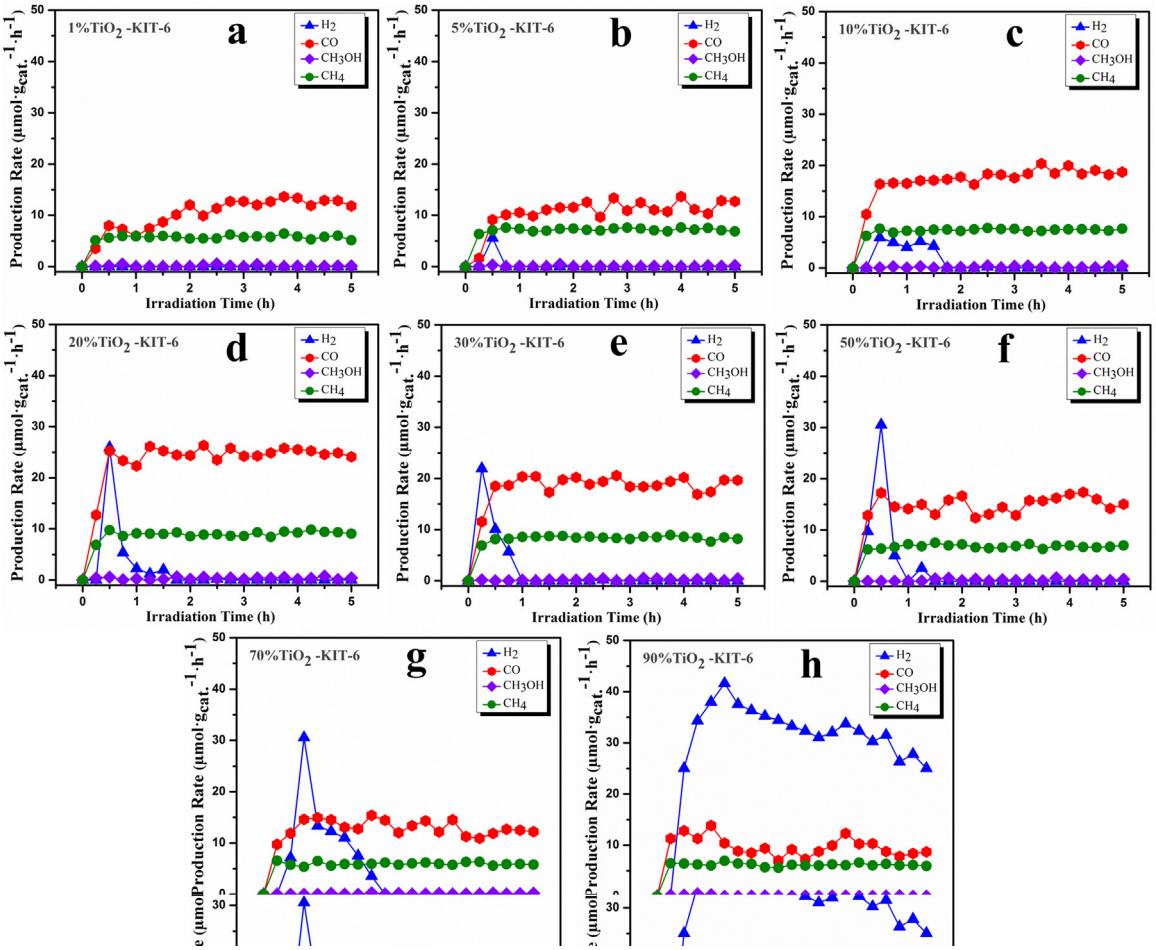

Fig. 9. Comparison of the photocatalytic production rates of the TiO_2(1–90%)/KIT-6 catalysts, under standard operating reaction conditions with 20% CO_2, 0.2 g of the photocatalyst, 50 mL/min flow rate, H_2O/CO_2 = 0.1, and 300 W UV lamp.

the TiO_2(90%)/KIT-6 photocatalyst. The better photocatalytic performance of TiO_2(20%)/KIT-6 than that of all the other catalysts, was due to the more uniform dispersion of TiO_2, the comparatively smaller nanoparticles, and to the more active anatase phase. The higher surface area and pore volume, ordered and the large pore size with a 3D pore structure in the TiO_2(20%)/KIT-6, all play a significant role in the better and uniform dispersion of the active sites on the support. A photocatalyst with more active sites and a higher surface area has better adsorption of water and carbon dioxide, which in turn, increases the reaction products [38,39]. Moreover, it has been observed, and already discussed on the basis of the FE-SEM and STEM results, that TiO_2 has different surface morphologies for different loadings on KIT-6. These different morphologies of the TiO_2 active phase create different surface effects; the adsorption of CO_2 in particular varies for different surfaces and structures, and this could significantly affect the whole reaction [40]. The higher surface area, the 3D pore size, the better uniform dispersion of 20% TiO_2 with its homogeneous morphology all lead to a synergistic adsorption effect and hence better overall activity. However, competitive adsorption takes place between CO_2 and H_2O, and this leads to the formation of different products and different selectivity; this will be discussed later on with the help of the reaction mechanism.

It has been observed that CO_2 reduction with H_2O using TiO_2 photocatalysts proceeds through a complex mechanism, as the reaction pathways depend specifically on the reaction conditions, and proceed through branching pathways that produce different products. For this reason, various mechanistic reaction schemes have been reported in the literature [1,6,14]. However, knowledge regarding the reaction mechanism is still not complete and further efforts are needed to understand it more clearly.

The thermodynamically stable and chemically inert nature of CO_2 is a huge hurdle to oxide or reduce it to produce useful intermediate chemicals under normal operating conditions. It has been found that a single electron reduction of CO_2 to an anion radical $^{\bullet}CO_2^-$ has a very strong negative electrochemical potential of −1.90 V. [41]. Therefore, from a thermodynamically point of view, it is not feasible to imagine that a photocatalyst could provide a single photogenerated electron to a CO_2 molecule. However, the standard potential of H_2O necessary to generate H_2 is much lower, and is therefore viable.

Although it is impossible to transfer a single photogenerated electron to a CO_2 molecule, it is comparatively easy to conduct the proton-assisted transfer of multiple electrons. In this way, H_2 and CO formation is favored, as they need lower numbers of electrons and protons, while CH_4 and CH_3OH require more electrons and protons and are difficult to form [42].

The best way of activating an inert CO_2 molecule to reduce it in order to obtain useful products is to adsorb it on the surface of any semiconducting material; and this results in lowering of its energy barrier [43]. Therefore, this work has focused in particular on the adsorption of CO_2 and H_2O on the surface of the photocatalysts. Fig. 11 shows the reaction mechanism, with the steps and pathways necessary to achieve the required energy-bearing products. Before starting the reaction, the CO_2 and H_2O vapors were adsorbed to obtain good adsorption of these reactants on the photocatalyst surface. However, H_2O, being a polar (1.85D) molecule,

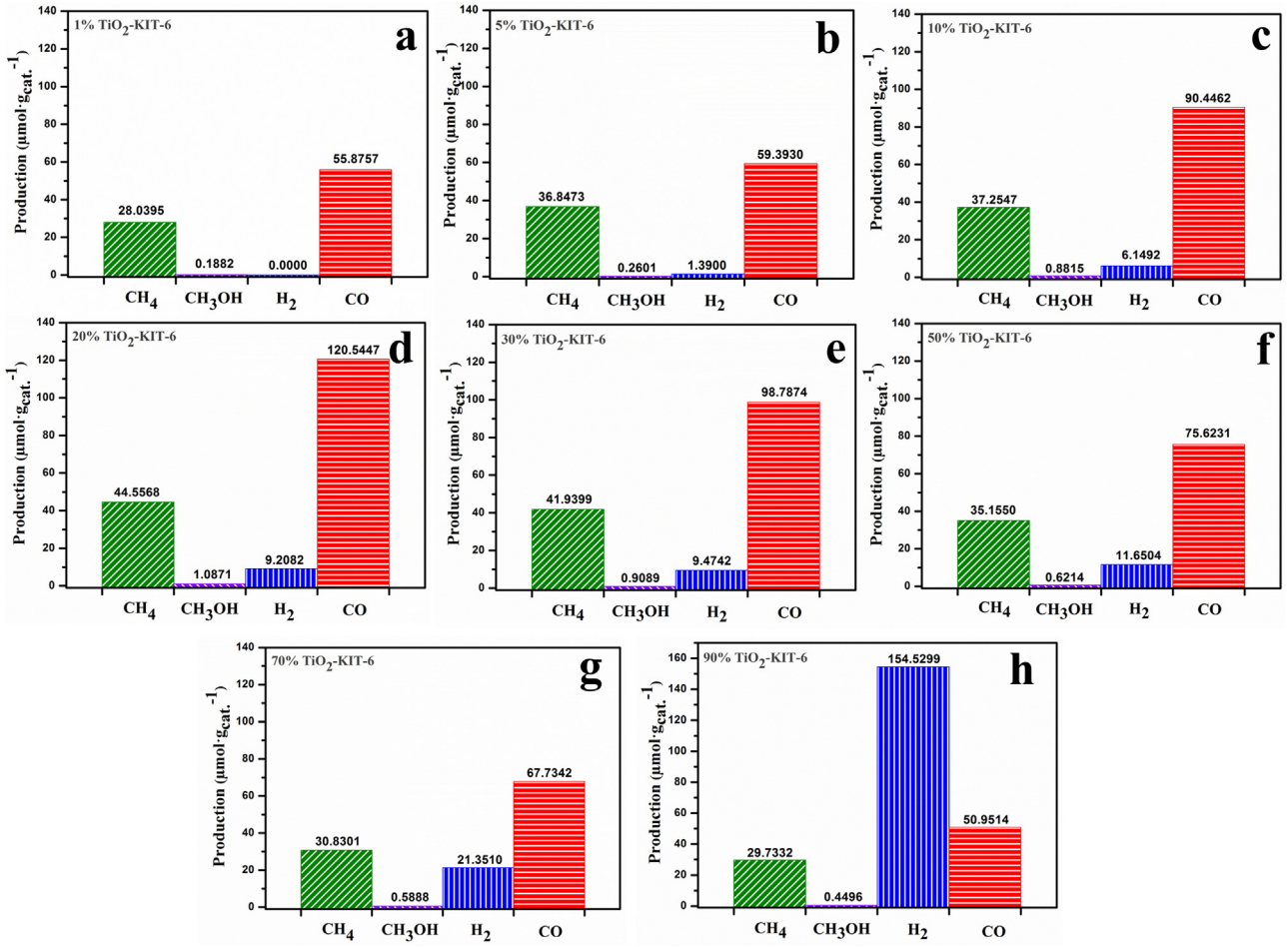

Fig. 10. Production comparison of the TiO_2(1–90%)/KIT-6 catalysts over a 5 h reaction time, under standard operating reaction conditions with 20% CO_2, 0.2 g of the photocatalyst, 50 mL/min flow rate, H_2O/CO_2 = 0.1, and 300 W UV lamp.

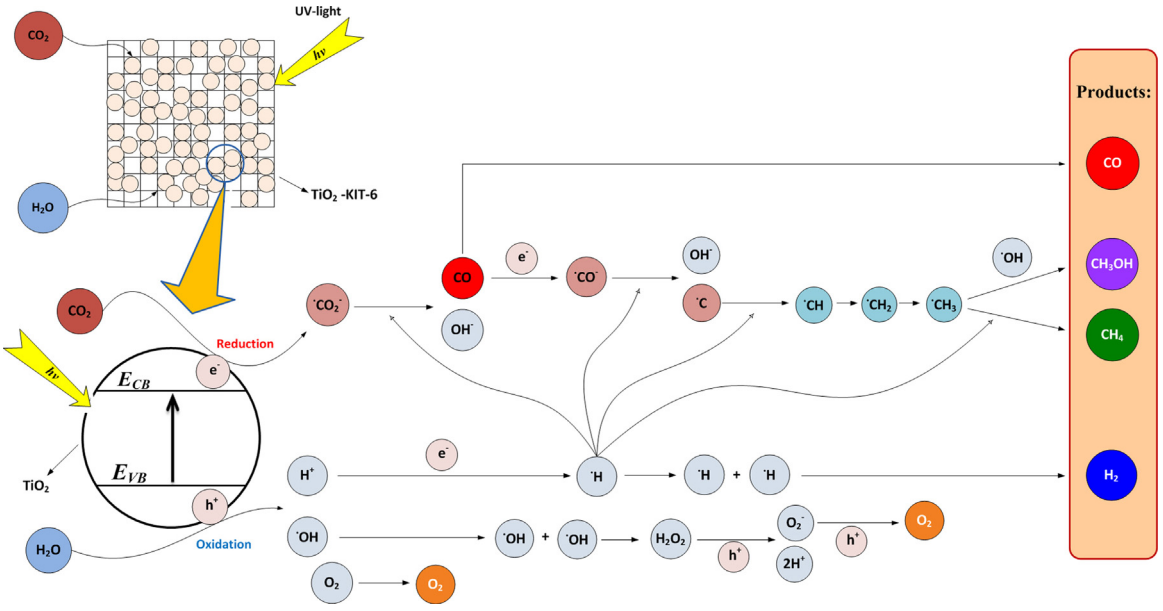

Fig. 11. The reaction mechanism and pathways of CO_2 reduction, with H_2O vapor, to various energy-bearing products by means of nanostructured TiO_2/KIT-6 photocatalysts.

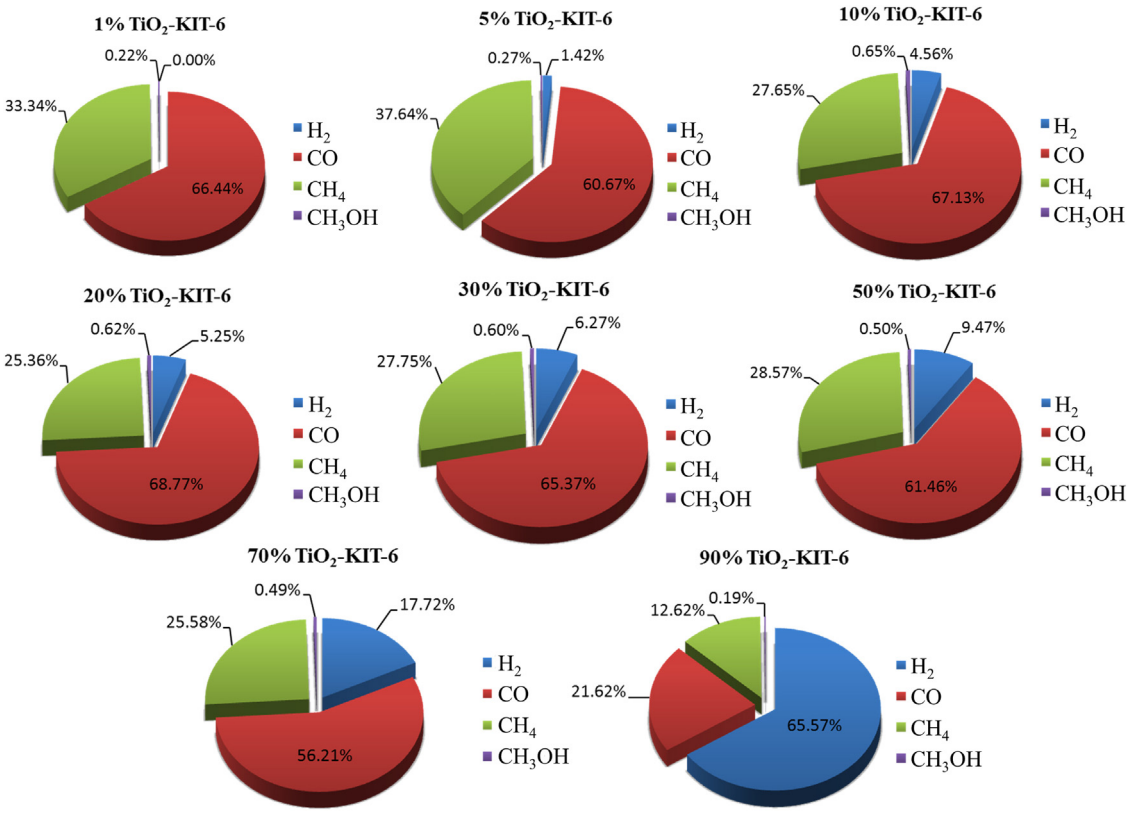

Fig. 12. Product selectivity comparison of the TiO_2(1–90%)/KIT-6 photocatalysts over a 5 h reaction time, under standard operating reaction conditions with 20% CO_2, 0.2 g of the photocatalyst, 50 mL/min flow rate, H_2O/CO_2 = 0.1, and 300 W UV lamp.

has more tendency to be adsorbed than CO_2, which has a lower dipole moment (0D); this indicates that both H_2O and CO_2 compete for adsorption on the active sites.

Moreover, as already mentioned different TiO_2 loadings dispersed on KIT-6 provide different dispersions, morphologies and thicknesses, and therefore provide different adsorption degrees of the reactants (CO_2, H_2O) on these photocatalytically active sites. As adsorption equilibrium is reached, electrons and holes are generated, upon UV irradiation, and the reaction initiates quickly, as shown in Fig. 11. Initially, electrons reach the adsorbed CO_2 molecules and reduce them to an anion radical $^{\bullet}CO_2^-$. In the meanwhile, H_2O oxidation initiates through the holes, produces H^+, $^{\bullet}OH$ or O_2 (desorbed) or participates further in the reaction to deactivate the photocatalyst, which will be discussed later on. In the next step, H^+ takes these electrons and forms $^{\bullet}H$, which eventually reacts with $^{\bullet}CO_2^-$ and produces CO and OH^-. The formation of CO in this reaction is an easy way to proceed, as can be observed in Figs. 9 and 10. The produced CO either desorbs as a product or is further reduced to $^{\bullet}C$, and then forms a chain reaction with $^{\bullet}H$ to generate $^{\bullet}CH$, $^{\bullet}CH_2$, or $^{\bullet}CH_3$. In an alternative pathway, two $^{\bullet}Hs$ combine together to produce H_2, which has been observed to be the highest by the TiO_2(90%)/KIT-6 photocatalyst; this might be due to the greater adsorption of H_2O, because of the higher hydrophilicity (90% TiO_2). Then $^{\bullet}CH_3$ further reacts with $^{\bullet}H$ to produce CH_4, while the $^{\bullet}OH$ obtained from the H_2O oxidation, either combines together to make O_2, or is directly utilized by $^{\bullet}CH_3$ to form CH_3OH as a product. The latter mechanism step, however, seems difficult and complex. Therefore, the best dispersion of the active sites, the good morphology, and lower hydrophilicity of TiO_2(20%)/KIT-6 might provide a comparatively better CO_2 and H_2O adsorption ratio, and therefore induce the overall reaction by accelerating the CO_2 reduction pathway to produce more CH_4, CH_3OH, and CO. The presence of active sites on the surface and within the mesostructure provides an additional benefit concerning the faster interfacial electron transfer from the photocatalyst to the gas molecules, which could increase the life of the electrons and holes and consequently lower the recombination of the photogenerated electron-hole pairs that could induce the overall reaction [44].

The reaction mechanism described in Fig. 11 clearly helps one to understand the selectivity of the products shown in Fig. 12. Lower TiO_2 loadings, from 1 to 20% on KIT-6, have shown good dispersion of the active phase and hence a better CO_2 adsorption induced CO_2 reduction pathway, which generally means better CH_4, CH_3OH, and CO selectivity. However, a further increase in TiO_2 loadings, from 30 to 90%, has been shown to gradually increase H_2O adsorption, and, as a result, to decrease the selectivity of CH_4, CH_3OH and CO, and gradually increase H_2 selectivity. Therefore, the described photocatalysts have selective ability, thus offering the opportunity of choosing an appropriate photocatalyst according to the specific requirements of producing a selective product, i.e., either CH_4, CH_3OH (hydrocarbons) or CO, H_2 (similar to syngas) for further applications.

Moreover, as shown in Fig. 13, the TiO_2(20%)/KIT-6 photocatalyst calcined at different calcination temperatures of 400–800 °C/3 h was further examined to obtain the best optimized state of the catalyst for its effective utilization in the reaction. As the calcination temperature was increased from 400 to 800 °C (Fig. 13a–e), the activity of the photocatalyst was decreased, in agreement with the characterization results, which showed more agglomerated TiO_2 for an increased rutile phase, and overall decreased physical characteristics of the catalyst calcined at higher temperatures. Therefore, TiO_2(20%)/KIT-6 calcined at 400 °C/3 h (Fig. 13a) can be considered the best condition for this application.

The final reaction test of the optimized TiO_2(20%)/KIT-6 photocatalyst was performed for an extended time of 24 h to observe the stability of the catalyst and the expected deactivation trend;

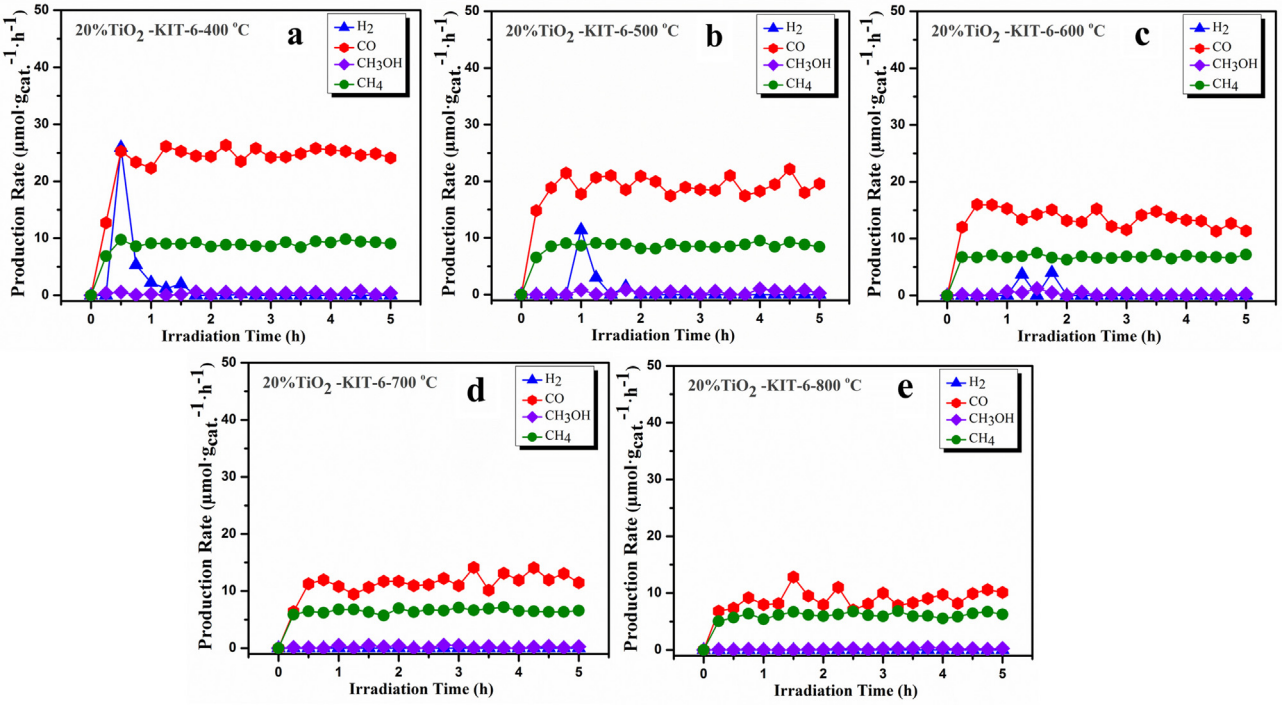

Fig. 13. Effect of the calcination temperature of the TiO_2(20%)/KIT-6 photocatalyst on the reaction activity, under standard operating reaction conditions, with 20% CO_2, 0.2 g of the photocatalyst, 50 mL/min flow rate, H_2O/CO_2 = 0.1, and 300 W UV lamp.

the results are shown in Fig. 14. It can be seen that the production rate of the main products, CH_4 and CO, was constant for 7 and 13 h of the reaction time, respectively. After these times, a gradually very slow deactivation was noticed. However, as shown in Fig. 14b, the yield of CH_4 and CO still increased even after 24 h of the reaction time. This stability was due to the high surface area of the photocatalyst, which provided good dispersion of the active TiO_2 phase as well as easy transportation of the reactants and products. The deactivation mechanism is not still clear, but with the passage of the reaction time, it could be due to the partial saturation of the active sites for adsorption on the photocatalyst surface with intermediate product/by-product/mixture formation. Moreover, after formation, some products such as CH_3OH and CO were considered not to have desorbed fully from the catalysts surface and were perhaps re-oxidized back into CO_2 through the produced O_2 (as reported in the reaction mechanism) during the reaction [45]. Therefore, a separate and in-depth focused study regarding these deactivating species in this photocatalyst is necessary in order to discover exact information about their nature and also to obtain a comprehensive understanding of the reaction mechanism that takes place during the reaction.

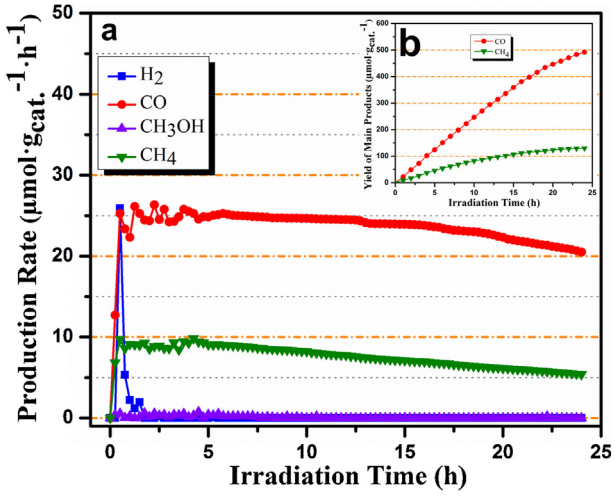

Fig. 14. Extended time activity test of nanostructured TiO_2(20%)/KIT-6 photocatalyst regarding the production rate and yield, under standard operating reaction conditions, with 20% CO_2, 0.2 g of the photocatalyst, 50 mL/min flow rate, H_2O/CO_2 = 0.1, and 300 W UV lamp.

4. Conclusions

Nanostructured TiO_2/KIT-6 photocatalysts with 1–90% TiO_2 loadings have been studied for CO_2 greenhouse gas reduction with H_2O vapor to produce various energy-bearing products, such as CH_4, CH_3OH (hydrocarbon), and CO, H_2 (similar to syngas). It has been found that different TiO_2 loadings on 3D ordered mesoporous silica, KIT-6, lead to the formation of different overall morphologies, phases, and physical properties, as well as the dispersion of the active sites. This has led to different adsorptions of the reactants (CO_2, H_2O) on these photocatalytically active sites. Hence, different production rates, yields and products have been obtained. Nanostructured TiO_2(20%)/KIT-6 has shown the highest photocatalytic performance, in terms of CH_4, CH_3OH and CO formation, due to the better physical characteristics, the uniformly dispersed TiO_2 on KIT-6, and greater CO_2 adsorption, due to the lower hydrophilicity. However, increases in TiO_2 loadings above 30% have shown non-uniform dispersion with particle agglomeration, which has led to a reduction in CH_4, CH_3OH, and CO formation and induced a H_2 production pathway. Therefore, TiO_2(90%)/KIT-6, which is equivalent to pure bulk TiO_2, has shown large agglomerates, light penetration limitations and more H_2O adsorption, due to the high hydrophilicity, as well as high selectivity toward H_2 formation. Moreover, the presence of active sites within the mesostructured KIT-6 high surface area material, has increased the overall reaction, because of the lower electron-hole pair recombination and has shown better catalytic stability. The long-term activity has shown

a gradually slow deactivation, due to partial saturation of the active sites by adsorption of the reactants/products, as well as the possibility of a re-oxidation back into CO_2 through the produced O_2.

However, the designed photocatalysts have shown ability toward various product selectivities, thus offering the opportunity of choosing an appropriate photocatalyst according to the requirements to produce a selected product, i.e., either CH_4, CH_3OH (hydrocarbons) or CO, H_2 (similar to syngas) for further applications. It can therefore be concluded that these nanostructured TiO_2/KIT-6 catalysts should be considered as promising and effective photocatalysts for CO_2 conversion to value-added energy-bearing products and as suitable candidates for further research activities.

Acknowledgement

The financial support from the Eco$^2CO_2$ European Project (309701-2 Eco$^2CO_2$ CP-FP FP7-NMP-2012-SMALL-6) is gratefully acknowledged.

Appendix A. Supplementary data

Supplementary data associated with this article can be found, in the online version, at http://dx.doi.org/10.1016/j.apcatb.2015.01.007.

References

[1] A. Kubacka, M. Fernandez-Garcia, G. Colon, Chem. Rev. 2 (2012) 1817–1828.
[2] S.C. Roy, O.K. Varghese, M. Paulose, C.A. Grimes, ACS Nano 4 (2010) 1259–1278.
[3] J.M. Melillo, A.D. Mcguire, D.W. Kicklighter, B. Moore, C.J. Vorosmarty, A.L. Schloss, Nature 363 (1993) 234–240.
[4] W.G. Tu, Y. Zhou, Z.G. Zou, Adv. Mater. 26 (2014) 4607–4626.
[5] N.A. Rashidi, S. Yusup, B.H. Hameed, Energy 61 (2013) 440–446.
[6] S.N. Habisreutinger, L. Schmidt-Mende, J.K. Stolarczyk, Angew. Chem. Int. Ed. 52 (2013) 7372–7408.
[7] A. Dhakshinamoorthy, S. Navalon, A. Corma, H. Garcia, Energy Environ. Sci. 5 (2012) 9217–9233.
[8] H. Shi, G. Chen, C. Zhang, Z. Zou, ACS Catal. 4 (2014) 3637–3643.
[9] V. Kumar, N. Labhsetwar, S. Meshram, S. Rayalu, Energy Fuels 25 (2011) 4854–4861.
[10] K. Huang, C.L. Sun, Z.J. Shi, Chem. Soc. Rev. 4 (2011) 2435–2452.
[11] I. Inoue, A. Fujishima, S. Konishi, K. Honda, Nature 277 (1979) 637–638.
[12] M. Hussain, P. Akhter, N. Russo, G. Saracco, Catal. Commun. 36 (2013) 58–62.
[13] O.K. Varghese, M. Paulose, T.J. LaTempa, C.A. Grimes, Nano Lett. 10 (2010) 750.
[14] K. Koci, L. Obalova, L. Matejova, D. Placha, Z. Lacny, J. Jirkovsky, O. Solcova, Appl. Catal. B: Environ. 89 (2009) 494–502.
[15] P. Akhter, M. Hussain, G. Saracco, N. Russo, Nanoscale Res. Lett. 9 (2014) 1–8.
[16] G. Qin, Y. Zhang, X. Ke, X. Tong, Z. Sun, M. Liang, S. Xue, Appl. Catal. B: Environ. 129 (2013) 599–605.
[17] M. Hussain, P. Akhter, N. Russo, G. Saracco, Chem. Eng. J. (2014), http://dx.doi.org/10.1016/j.cej.2014.08.095.
[18] G.A. Andrade, A.J. Pistner, G.P.A. Yap, D.A. Lutterman, J. Rosenthal, ACS Catal. 3 (2013) 1685–1692.
[19] P. Akhter, M. Hussain, G. Saracco, N. Russo, Fuel (2014), http://dx.doi.org/10.1016/j.fuel.2014.09.079.
[20] W. Hou, W.H. Hung, P. Pavaskar, A. Goeppert, M. Aykol, S.B. Cronin, ACS Catal. 1 (2011) 929–936.
[21] D. Uner, M.M. Oymak, Catal. Today 181 (2012) 82–88.
[22] O. Ozcan, F. Yukruk, E.U. Akkaya, D. Uner, Appl. Catal. B: Environ. 71 (2007) 291–297.
[23] H. Yamashita, Y. Fujii, Y. Ichihashi, S.G. Zhang, K. Ikeue, D.R. Park, K. Koyano, T. Tatsumi, M. Anpo, Catal. Today 45 (1998) 221–227.
[24] M. Hussain, D. Fino, N. Russo, J. Hazard. Mater. 211–212 (2012) 255–265.
[25] K. Soni, B.S. Rana, A.K. Sinha, A. Bhaumik, M. Nandi, M. Kumar, G.M. Dhar, Appl. Catal. B: Environ. 90 (2009) 55–63.
[26] M. Hussain, D. Fino, N. Russo, Chem. Eng. J. 238 (2014) 198–205.
[27] D.R. Sahu, L.Y. Hong, S.-C. Wang, J.-L. Huang, Micropor. Mesopor. Mater. 117 (2009) 640–649.
[28] T.L. Thompson, J.T. Yates, Chem. Rev. 106 (2006) 4428–4453.
[29] M.A.A. Aziz, A.A. Jalil, S. Triwahyono, R.R. Mukti, Y.H. Taufiq-Yap, M.R. Sazegar, Appl. Catal. B: Environ. 147 (2014) 359–368.
[30] M. Hussain, N. Abbas, D. Fino, N. Russo, Chem. Eng. J. 188 (2012) 222–232.
[31] K. Kaneko, J. Membr. Sci. 96 (1994) 59–89.
[32] M. Hussain, N. Russo, G. Saracco, Chem. Eng. J. 166 (2011) 138–149.
[33] J.T. Carneiro, T.J. Savenije, J.A. Moulijn, G. Mul, J. Phys. Chem. C 115 (2011) 2211–2217.
[34] M. Hussain, R. Ceccarelli, D.L. Marchisio, D. Fino, N. Russo, F. Geobaldo, Chem. Eng. J. 157 (2010) 45–51.
[35] A. Fujishima, K. Hashimoto, T. Watanabe, TiO_2 Photocatalysis: Fundamentals and Applications, English ed., BKC Inc., Tokyo, 1999.
[36] A.Y. Stakheev, E.S. Shpiro, J. Apijok, J. Phys. Chem. 97 (1993) 5668–5672.
[37] L. Collado, P. Jana, B. Sierra, J.M. Coronado, P. Pizarro, D.P. Serrano, V.A.D. O'Shea, Chem. Eng. J. 224 (2013) 128–135.
[38] J.C.S. Wu, H.M. Lin, C.L. Lai, Appl. Catal. A: Gen. 296 (2005) 194–200.
[39] G. Liu, N. Hoivik, K. Wang, H. Jakobsen, Sol. Energy Mater. Sol. Cells 105 (2012) 53–68.
[40] U. Burghaus, Catal. Today 148 (2009) 212–220.
[41] M. Cokoja, C. Bruckmeier, B. Rieger, W.A. Herrmann, F.E. Kuhn, Angew. Chem. Int. Ed. 50 (2011) 8510–8537.
[42] N.M. Dimitrijevic, B.K. Vijayan, O.G. Poluektov, T. Rajh, K.A. Gray, H.Y. He, J. Am. Chem. Soc. 133 (2011) 3964–3971.
[43] V.P. Indrakanti, J.D. Kubicki, H.H. Schobert, Energy Environ. Sci. 2 (2009) 745–758.
[44] M.R. Hoffmann, S.T. Martin, W.Y. Choi, D.W. Bahnemann, Chem. Rev. 95 (1995) 69–95.
[45] Y. Li, W.N. Wang, Z.L. Zhan, M.H. Woo, C.Y. Wu, P. Biswas, Appl. Catal. B: Environ. 100 (2010) 386–392.